6130 *Chem. Mater.* **2010,** *22,* 6130–6137
DOI:10.1021/cm101741n

CHEMISTRY OF MATERIALS
Article

$ZnFe_2O_4$ Nanoparticles: Different Magnetic Behavior When They Are Hosted in Porous Structures

V. Blanco-Gutiérrez, E. Urones-Garrote, María J. Torralvo-Fernández, and R. Sáez-Puche*

Departamento de Química Inorgánica, Facultad de Ciencias Químicas, Universidad Complutense, Ciudad Universitaria, 28040 Madrid, Spain

Received June 22, 2010. Revised Manuscript Received October 7, 2010

$ZnFe_2O_4$ nanoparticles have been prepared encased into sepiolite and faujasite matrixes. Transmission electron microscopy (TEM) images show hosted particles from 1 to 3 nm. From the zero field cooling (ZFC) and field cooling (FC) magnetic susceptibility data, the blocking temperatures distribution has been obtained, which reflects the particle size distribution. In both samples, the particles seem to present two well-defined sizes. Taking into account the adsorption results, the smallest particles must be located in the micropores of the sepiolite and faujasite structures, while the largest ones are probably hosted in structural defects. On the other hand, when the thermal energy overcomes the anisotropy barrier, at temperatures higher than T_B, the abrupt decreasing of magnetization observed in the ZFC and FC curves would indicate that the hosted nanoparticles are free to rotate. This leads one to believe that they do not present any mechanical impediment that could avoid their free rotation. This fact can be attributed to the good dispersibility of the nanoparticles in the matrixes, which implies noninteracting particles, and to the negligible interaction with the surface of the cavities.

1. Introduction

Magnetic nanoparticles have drawn a great deal of attention over the past years because they present different physical properties with respect to bulk materials with the same composition.[1] Their magnetic behavior displays some unique features, such as superparamagnetism which is one of the most studied finite size effects.[2,3]

As other spinel ferrites, the $ZnFe_2O_4$ compound at the nanoscale presents rich crystal chemistry and its magnetic properties vary greatly with the chemical structure which depends on the particle size and synthesis conditions.[4,5] In this sense, microscopic Zn-ferrite behaves as antiferromagnetic with a $T_{Néel} = 10$ K[6] as a result of the cationic distribution in the normal spinel structure $(Zn)[Fe]_2O_4$ in which Zn^{2+} cations tend to occupy the tetrahedral sites (A) whereas the Fe^{3+} cations occupy the octahedral (B) ones. This results in the formation of two Fe^{3+} sublattices with opposite magnetic moment giving a zero net moment. However, nanoscaled Zn-ferrite seems to be partially inverted $(Zn_{1-x}Fe_x)[Fe_{2-x}Zn_x]O_4$ where part of the Zn^{2+} cations are located in the B sites and Fe^{3+} cations in the A sites.[7] Because of this different cation distribution, the Fe^{3+} sublattices are decompensated and consequently it has ferrimagnetic behavior below a certain temperature called the blocking temperature (T_B).[8] Above the T_B, as the nanoparticles are single-domain, they show superparamagnetic behavior with the absence of a coercive field.[9−11]

Nowadays, all the efforts are focused on developing effective methods for synthesizing ferrite nanoparticles with controlled size and shape in order to tailor their magnetic properties.[12−14] It has been found that uniform pore structures can be effective reaction vessels to obtain confined nanoparticles with uniform size as the pore matrix imposes an upper limit on the particle size.[15] They also avoid the particle agglomeration and offer a homogeneous dispersibility inside them. Several inorganic matrixes are used as porous hosts of magnetic nanoparticles, such as cross-linked polymer resins[16] or inorganic molecular sieves as zeolites.[17] Unlike the polymeric matrixes,

*To whom correspondence should be addressed. E-mail: rsp92@quim.ucm.es.

(1) Goya, G. F.; Rechenberg, H. R. *J. Magn. Magn. Mater.* **1999**, *196−197*, 191.
(2) Batlle, X.; Labarta, A. *J. Phys. D: Appl. Phys.* **2002**, *35*, R15.
(3) Tartaj, P. *Eur. J. Inorg. Chem.* **2009**, 333.
(4) Oliver, S. A.; Harris, V. G.; Hamdeh, H. H.; Ho, J. C. *Appl. Phys. Lett.* **2000**, *76*(19), 2761.
(5) Hamdeh, H. H.; Ho, J. C. *Phys. Rev. B* **1999**, *60*(5), 3400.
(6) Hastings, J. M.; Corliss, L. M. *Phys. Rev.* **1956**, *102*(6), 1460.
(7) Nachbaur, V.; Tauvel, G.; Verdier, T.; Jean, M.; Juraszek, J.; Houvet, D. *J. Alloys Compd.* **2009**, *473*, 303.
(8) Chinnasamy, C. N.; Narayanasamy, A.; Ponpandian, N.; Chattopadhyay, K. *Mater. Sci. Eng., A* **2001**, *A304−306*, 983.
(9) Lu, A. H.; Salabas, E. L.; Schüth, F. *Angew. Chem., Int. Ed.* **2007**, *46*, 1222.
(10) Petracic, O. Superlattices Microstruct. **2010**, DOI:10.1016/j.spmi.2010.01.009.
(11) Vejpravová, J. P.; Schovský, V. WDS'05 Proceedings of Contributed Papers, Part III, **2005**; p 518.
(12) Liu, C.; Zhang, Z. J. *Chem. Mater.* **2001**, *13*, 2092.
(13) Song, Q.; Zhang, Z. J. *J. Am. Chem. Soc.* **2004**, *126*, 6164.
(14) Sun, S.; Zeng, H. *J. Am. Chem. Soc.* **2002**, *124*, 8204.
(15) Pierella, L. B.; Saux, C.; Bertorello, H. R.; Bercoff, P. G.; Botta, P. M.; Rivas, J. *Mater. Res. Bull.* **2008**, *43*, 2026.
(16) Smith, G. D.; Bedrov, D. *Langmuir* **2009**, *25*(19), 11239.
(17) Bertorello, H. R.; Pierella, L. B.; Bercoff, P. G.; Saux, C.; Sinnecker, J. P. *Phys. B* **2004**, *354*, 137.

 Published on Web 10/20/2010

most of the zeolitic ones are chemically inert and biocompatible which makes them good candidates to be used as a coating of oxide nanoparticles. Thanks to this, they can be useful for drug-delivery, as magnetic contrast agents in magnetic resonance imaging (MRI), as hyperthermia agents, or as magnetic vectors that can be directed to a specific body region by means of a magnetic field.[18−21] On the other hand, as we describe in a previous work,[22] when a solid matrix is used to disperse the nanoparticles, it precludes them from any local movement when a magnetic field is applied, as they are firmly embedded to it. However, it has been found that it is possible to obtain the opposite phenomenon, that is, a composite of rotationally free nanoparticles encased in the cavities of the zeolitic matrix.[23] This remarkable fact makes these new materials present potential applications as electronic devices, ferrofluids, electrooptic materials, catalysts, biomedical materials, or pigments.

In most of the studied nanocomposites, the entrapped particles are metallic or simple metal oxide,[24,25] but in this work we explain the obtaining of novel nanocomposites formed by confined mixed oxide nanoparticles. The aim is to study the magnetic behavior of $ZnFe_2O_4$ nanoparticles entrapped in the pore structure of two inorganic matrixes, sepiolite and faujasite that have been found to present an appropiate pore diameter to obtain nanoparticles inside them by an easy synthesis method. Sepiolite ($Mg_8Si_{12}O_{30}(OH)_4(H_2O)_4 \cdot 8H_2O$) particles have a needlelike morphology. The structure consists of two layers of tetrahedral Si^{4+} connected by oxygen atoms to a central discontinuous layer of octahedral coordinated Mg^{2+}. This arrangement results in parallel channels of 1.3 nm × 0.67 nm in which there are water molecules and hydroxil ions. The loss of four water molecules per unit cell leads to the folding of the crystal structure,[26] which is reversible if the dehydration occurs below 400 °C.[27] This particular feature could be useful when the entrapped nanoparticles are wanted to be released. The faujasite framework $(Na_2,Ca,Mg)_{3.5}[Al_7Si_{17}O_{48}] \cdot 32(H_2O)$ consists of parallel arrangements of 1.3 nm diameter supercages which are formed by 10 sodalite units. These supercages are accessible through 0.74 nm diameter windows.[28]

2. Experimental Section

Preparation of Zn-Ferrite Nanoparticles Encapsulated in Sepiolite Fibers. Pangel sepiolite fibers (sample S) were supplied by the TOLSA Company. First, two portions of this material were dehydrated in air at 200 °C during 12 h (sample S200) and 350 °C during 5 h (sample S350) according to the TG-curve (see the Supporting Information). Afterward, 0.15 g of S350 sample were put into 8 mL of a previously melted at 80 °C mixture of zinc and iron nitrates with a molar ratio Zn/Fe of 1:2 during 12 h. The brown solid was then recovered after filtering and washing with ethanol and kept under ammonia atmosphere during 7 h to obtain the hydroxide precursors of the ferrite compound. Afterward, the sepiolite with the embedded precursors of the ferrite was transferred into a Teflon stainless steal autoclave with a third of its volume filled with ethylene glycol and treated at 160 °C during 18 h. The obtained sample was called SZn. Additionally, samples S200 and S350 were subjected to the same solvothermal treatment as sample SZn but without the embedded precursors. The obtained samples were named S200s and S350s, respectively.

Preparation of Zn-Ferrite Nanoparticles Encapsulated in Faujasite Crystals. The faujasite was synthesized as follows. The precursor gel of this zeolite was prepared with the molar ratio 10 SiO_2/2.3 Al_2O_3/5.5 $(TMA)_2O$/0.06 Na_2O/570 H_2O.[29]

The chemicals were purchased from Aldrich and used without further purification. A tetramethylammonium hydroxide solution was prepared with approximately 25% of the needed distilled water. This solution was added to an aluminum isopropoxide solution made with the rest of the needed distilled water. After 1 h stirring, silica suspensions LUDOX HS40 and LUDOX AS40 were added consecutively. The resulting mixture was stirred for 1 h and aged at 25 °C during 10 days. Afterward, the obtained gel was transferred into an autoclave to be hydrothermally treated at 100 °C during 7 days. The obtained white product was then centrifuged, washed with distilled water, and dried at room temperature.

The obtained faujasite was then outgassed by gradually increasing the temperature (∼1 °C/h) from 20 to 167 °C under dynamic vacuum. Every 10 °C increasing temperature, the faujasite was kept at that temperature and $\approx 1 \times 10^{-4}$ Torr during 24 h. The obtained sample was called F. Afterward, 0.15 g of previously outgassed faujasite (F sample) were put into 8 mL of a $ZnCl_2$ and $FeSO_4 \cdot 7H_2O$ 0.165 M solution with a molar ratio Zn/Fe 1:2. After 20 min, the mixture was filtered and washed with ethanol. The recovered solid was then put under ammonia atmosphere during 2 h and later transferred into an autoclave with a third of its volume filled with ethylene glycol. The mixture was treated at 100 °C during 20 h and afterward filtered, washed with ethanol, and dry at room temperature. The obtained sample was called FZn.

It was also prepared another sample named Fs which was obtained in similar conditions as those used in the preparation of FZn sample: 0.15 g of faujasite (F sample) were mixed with 8 mL of HCl solution of pH = 5. After 20 min, the solid was filtered and washed with ethanol to put it afterward in ammonia atmosphere for 2 h. Finally, the white solid was transferred into an autoclave with a third of its volume filled with ethylene glycol to be treated at 100 °C during 20 h.

Preparation of Zn-Ferrite Nanoparticles Nonincorporated to a Matrix. They were prepared with a similar size to those nanoparticles encapsulated in the sepiolite and faujasite matrixes in

(18) Arruebo, M.; Fernandez-Pacheco, R.; Ibarra, M. R.; Santamaría, J. *Nanotoday* **2007**, *2*(3), 22.
(19) Weinstein, J. S.; Varallyay, C. G.; Dosa, E.; Gahramanov, S.; Hamilton, B.; Rooney, W. D.; Muldoon, L. L.; Neuwelt, E. A. *J. Cereb. Blood Flow Metab.* **2010**, *30*, 15.
(20) Cassim, S. M.; Giustini, A. J.; Petryk, A. A.; Strawbridge, R. A.; Hoopes, P. J. *Proc. SPIE* **2009**, *7181*, 71810O.
(21) Laurent, S.; Forge, D.; Port, M.; Roch, A.; Robic, C.; Vander Elst, L.; Muller, R. N. *Chem. Rev.* **2008**, *108*, 2064.
(22) Blanco-Gutierrez, V.; Torralvo-Fernandez, M. J.; Saez-Puche, R. *J. Phys. Chem. C* **2010**, *114*(4), 1789.
(23) Tejada, J.; Zhang, X. X.; Kroll, E.; Bohigas, X.; Ziolo, R. F. *J. Appl. Phys.* **2000**, *87*(11), 8008.
(24) Hincapie, B. O.; Garces, L. J.; Gomez, S.; Ghosh, R.; Suib, S. L. *Catal. Today* **2005**, *110*(3−4), 323.
(25) Bouvy, C.; Marine, W.; Sporken, R.; Su, B. L. *Colloids Surf. A: Physicochem. Eng. Aspects* **2007**, *300*, 145.
(26) Grillet, Y.; Cases, J. M.; Francois, M.; Rouquerol, J.; Poirier, J. E. *Clays Clay Miner.* **1988**, *36*(3), 233.
(27) Ruiz, R.; del Moral, J. C.; Pesquera, C.; Benito, I.; Gonzalez, F. *Thermochim. Acta* **1996**, *279*(1−2), 103.
(28) Lim, W. T.; Seo, S. M.; Kim, G. H.; Lee, H. S.; Seff, K. *J. Phys. Chem. C* **2007**, *111*, 18294.
(29) Fan, W.; Shirato, S.; Gao, F.; Ogura, M.; Okubo, T. *Microporous Mesoporous Mater.* **2006**, *89*, 227.

order to compare their magnetic behavior. Stoichiometric amounts of zinc and iron nitrates were dissolved in 10 mL of ethylene glycol in a 10^{-4} mol/ml concentration. Afterward, KOH 2 M was added until pH = 11. The mixture was then transferred into an autoclave and treated at 160 °C for 2 h.[22] This sample was called Zn3.

Characterization Techniques. The structural phases were identified by X-ray diffraction using a Siemens D-5000 powder diffractometer (25 mW, 35 kV) with a radiation Cu Kα. Morphology and size of the particles were characterized by transmission electron microscopy (TEM) employing a JEOL-2000FX microscope working at 200 kV and scanning transmission electron microscopy (STEM) using a JEOL-3000F microscope working at 300 kV. Magnetic properties were measured using a Quantum Design XL-SQUID magnetometer in the temperature range of 2−300 K up to 5 T. Magnetic susceptibility was measured after cooling the sample at 2 K in zero field cooling (ZFC) and applying afterward a magnetic field of 500 Oe. In the case of field cooling measurements (FC), the sample was cooled in presence of a 500 Oe field down to 2 K. Textural characterization was done with a surface area analyzer ASAP 2020 from Micromeritics. Prior to the measurements, the samples were outgassed at 110 °C and ≈1×10^{-3} Torr for 2 h. The Brunauer−Emmett−Teller (BET) equation was used to calculate the surface area and the external surface and micropore volume was determined using the *t*-plot.[30] The mesopore size distributions were calculated using the Barrett−Joyner−Halenda (BJH) method for a cylindrical pore mode.[31] Micropore size distributions were calculated using the Horvath−Kawazoe equation.[32]

3. Results and Discussion

Because of the small size of the encapsulated nanocrystals, the intensities of their reflections must be very low compared to the matrixes' ones and therefore the X-ray diffraction patterns of samples SZn and FZn samples (not shown) only present the reflection maxima corresponding to the sepiolite and faujasite, respectively. This has already been observed by other authors in several cases.[33,34]

TEM images of natural sepiolite and synthesized faujasite are shown in Figure 1a and 2a, respectively. The observed dark dots in SZn and FZn samples (Figures 1b and 2b, respectively) probably correspond to the encased nanoparticles but could also correspond to some structural defects created during the solvothermal treatment as the images of samples S350s and Fs seem to indicate (see the Supporting Information). On the other hand, X-ray energy dispersive spectroscopy (XEDS) analyses were done to SZn and FZn samples, revealing in both cases a ratio Fe/Zn in agreement with the stoichiometry 2:1 of the Zn ferrite compound (see Figure 2e in the case of the FZn sample). On the other hand, inductively coupled plasma (ICP) analyses of FZn sample also reveals a 2:1 Fe/Zn molar ratio and an estimated ferrite weight content of 8%.

In the electron diffraction pattern of SZn (inset Figure 1b) and FZn samples, it is difficult to identify the intensities corresponding to the spinel phase of the ferrite nanoparticles as their intensities are very low, diffuse, and very close to the sepiolite and faujasite maxima. In the electron diffraction pattern of the SZn sample (inset Figure 1b), some diffraction maxima that agree with the, 311, 440, and 511 reflections of the spinel phase are marked with an F.

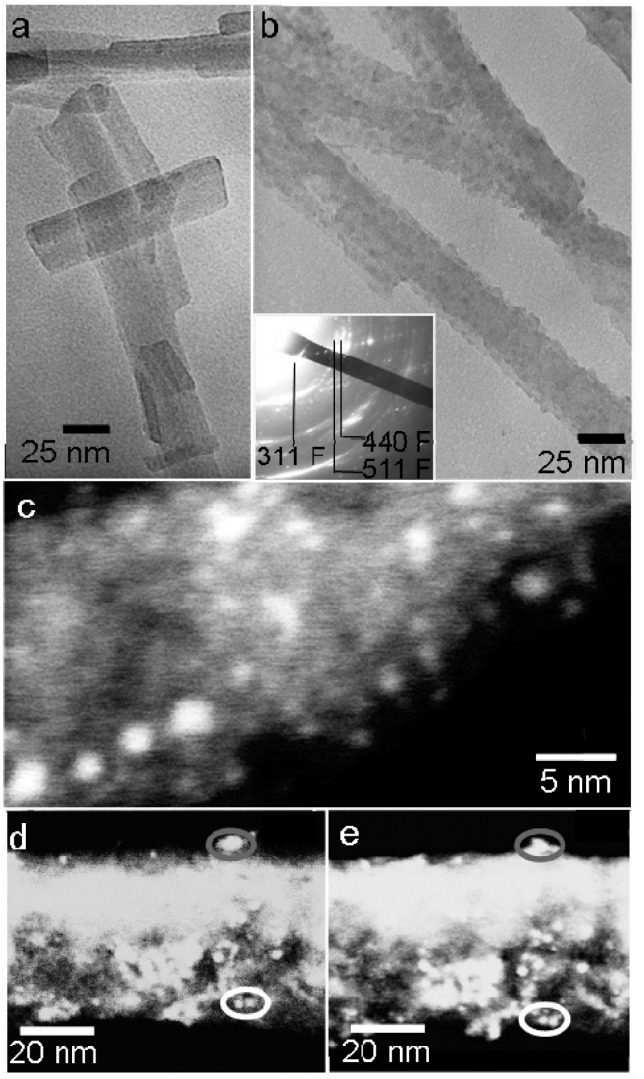

Figure 1. TEM images of S (a) and SZn (b) samples. STEM images of SZn sample are shown in parts c−e.

STEM images shown in Figures 1c−e and 2c clearly show the encapsulated nanoparticles in both sepiolite and faujasite matrixes, respectively, that appear as the brightest dots. These STEM images also reveal that homogeneous particle size and shape for the encased nanoparticles were obtained for both the SZn and FZn samples. The mean ferrite particle size in these nanocomposites obtained after statistical analysis from STEM images by measuring 100 nanoparticles was 1−3 nm. It is worth noting as well that the nanoparticles are aligned inside the matrixes as it can be observed. The STEM images taken before and after the rotation of a SZn fiber (Figure 1d,e) reveal that most of the Zn ferrite nanoparticles are inside the matrix and not in the fiber surface as they remain in the fiber projection for any rotation angle (see nanoparticles marked with a white circle), and only few of them are not inside but in the

(30) Harkins, W. D.; Jura, G. *J. Chem. Phys.* **1943**, *11*, 431.
(31) Barret, E. P.; Joyner, L. G.; Halenda, P. P. *J. Am. Chem. Soc.* **1951**, *73*, 373.
(32) Rege, S. U.; Yang, R. T. *AIChE J.* **2000**, *46*(4), 734.
(33) Iacomi, F. *Surf. Sci.* **2003**, *532−535*, 816.
(34) Chen, J.; Feng, Z.; Ying, P.; Li, C. *J. Phys. Chem. B* **2004**, *108*, 12669.

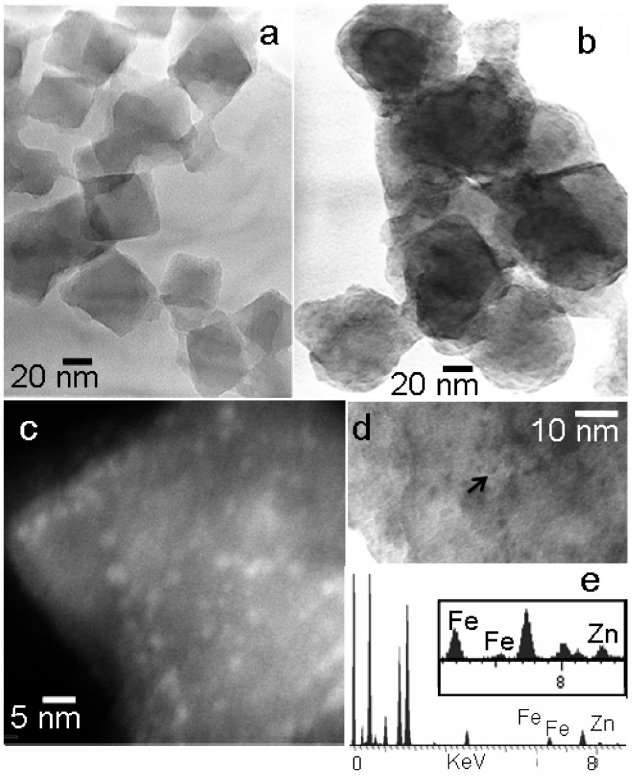

Figure 2. TEM images of F (a) and FZn (b,d) sample. STEM image of FZn sample is shown in part c. XEDS analysis of the FZn sample is shown in part e.

surface of the fiber (nanoparticles marked with a gray circle).

The nitrogen adsorption−desorption isotherms of sepiolite (samples S and S200) and faujasite (sample F) are plotted in Figures 3a and 4a. In the low pressures region, the isotherms show type I character as it is expected due to the microporous network of both materials. The higher values of adsorbed volume for S200 with respect to the S sample (Figure 3a inset) indicates the proper outgassing of the sepiolite channels after treatment at 200 °C. Moreover, the hysteresis loops that appear in the high pressure region indicate capillary condensation in mesopores that probably correspond to structural defects and interparticle holes. The textural parameters are collected in Table 1. S_t and V_m are the external surface and micropore volume, respectively, obtained from the *t*-plots. These V_m values are in agreement with the cumulative micropore volume calculated for each sample using the Horvath−Kawazoe equation (not shown). V_p is the cumulative mesopore volume obtained by the BJH method. In this table are also collected the textural parameters corresponding to the sepiolite treated at 350 °C and under solvothermal conditions (samples S350, S200s, and S350s). These three samples present similar values of S_{BET} which are also similar to the external surfaces and are one-half of the S_{BET} for the S200 sample. These results are in agreement with previous work and reflect the sepiolite structural folding.[26] It is known that the elimination of the water molecules bounded to the Mg^{2+} cations at temperatures higher than 350 °C results in the folding of the structure and therefore the structural channels are unavailable to

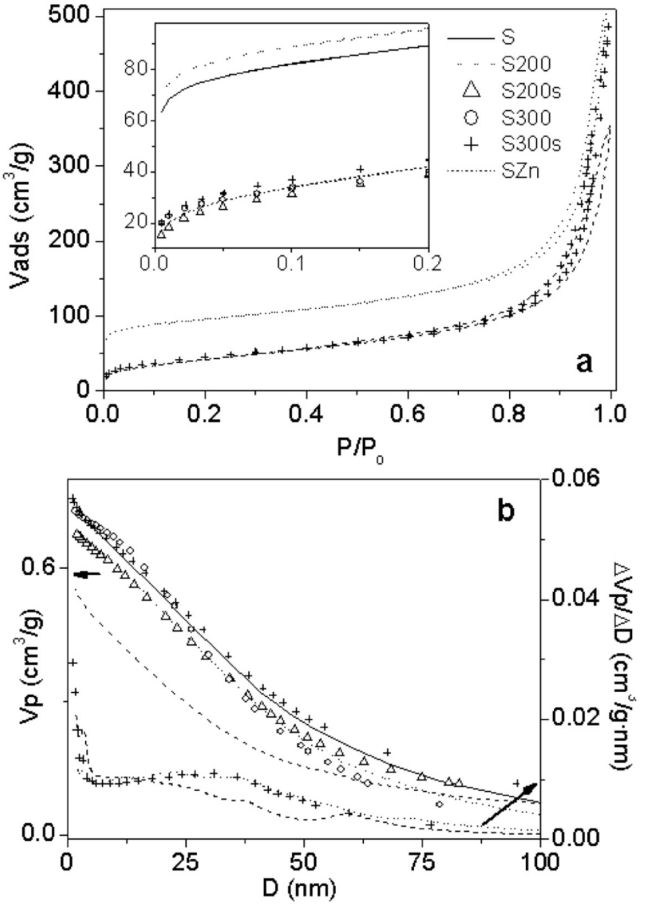

Figure 3. Isotherms (a), cumulative mesopore volume, and pore size distribution (b) for sepiolite samples.

the N_2 molecules.[26] According to that, the micropore volume of sample S350 is negligible (Table 1). The isotherm of S200s sample (Figure 3a inset) and the corresponding micropore volume seems to indicate that the folding also occurs during the solvothermal treatment even at 200 °C. Taking into account that in the preparation of the SZn sample the sepiolite was outgassed at 350 °C before the infiltration of the metal nitrates, the dehydroxilation of the sepiolite channels would have taken place at this temperature causing the folding structure. However, the folding is reversible when the temperature of treatment is lower than 400 °C[27] such that, when the sepiolite is added to the metal-nitrates solution it is rehydrated and it recuperates its initial morphology, being then the channels of the structure accessible to the ferrite precursors. In the afterward solvothermal treatment, the structure folds again and consequently the nanoparticles remain trapped in the cavities. In the SZn sample there are as well ferrite nanoparticles with a size of 1−3 nm (Figure 1c−e) which must be located in larger pores. In Figure 3b is plotted the cumulative mesopore volume as a function of the pore diameter for the different sepiolite samples and the size distributions for samples S200, S350s, and SZn. These pore size distributions are very broad and probably correspond to interparticular holes and structural defects. In the V_p vs *D* plot, it can be seen that all the samples show similar values of V_p except the SZn sample that presents

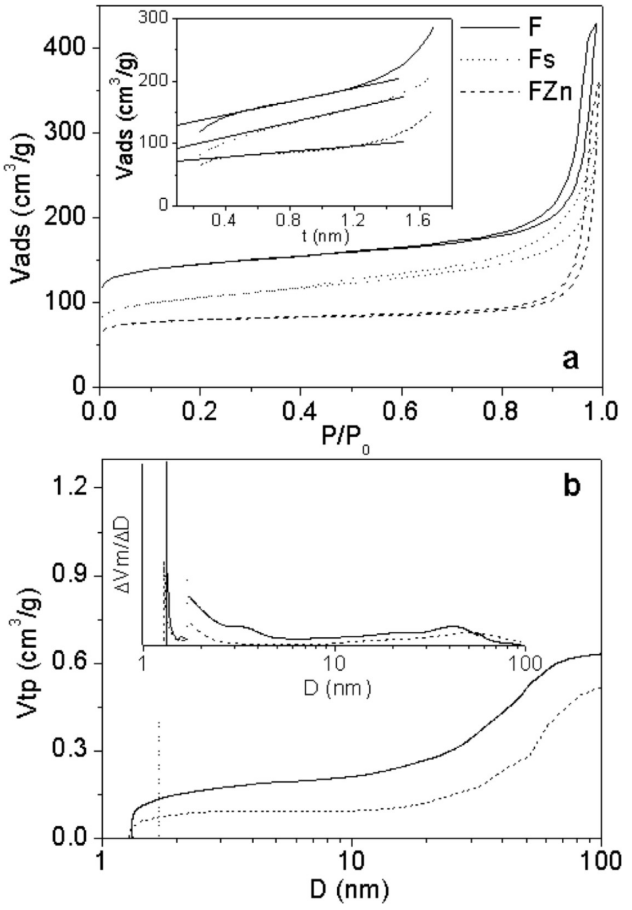

Figure 4. Isotherms (a) and *t*-plots (inset) for faujasite samples. Cumulative pore volume (b) and pore size distributions (inset) corresponding to the micropore and mesopore regions. Both ranges of the pores have been separated by a dotted line.

Table 1. Textural Parameters for Sepiolite and Faujasite Samples

sample	S_{BET} (m^2/g)	S_t (m^2/g)	V_p (cm^3/g)	V_m (cm^3/g)
S	299	155	0.75	0.070
S200	330	151	0.69	0.083
S200s	145	133	0.65	0.003
S350	141	126	0.7	0.007
S350s	162	149	0.72	0.003
SZn	156	145	0.52	0.004
F	516	78	0.50	0.177
Fs	350	87	0.38	0.136
FZn	258	22	0.45	0.070

lower values for mesopores with a diameter smaller than 50 nm (see also Table 1). This fact suggests that the ferrite nanoparticles are hosted in the structural defects.

The isotherms of FZn and Fs samples are also depicted in Figure 4a. The last one corresponds to the faujasite without the embedded ferrite precursors and treated in similar conditions to those used in the preparation of FZn sample. Compared to the F and Fs samples, FZn presents lower value of surface area due in part to the lower micropore volume as the *t*-plots (Figure 4a inset) and the V_m values in Table 1 indicate. For the as-synthesized faujasite (F sample) and faujasite with encased nanoparticles (FZn sample), the total cumulative pore volume (V_{tp}) that includes the cumulative micropore volume calculated using the Horvath−Kawazoe method and the mesopore volume

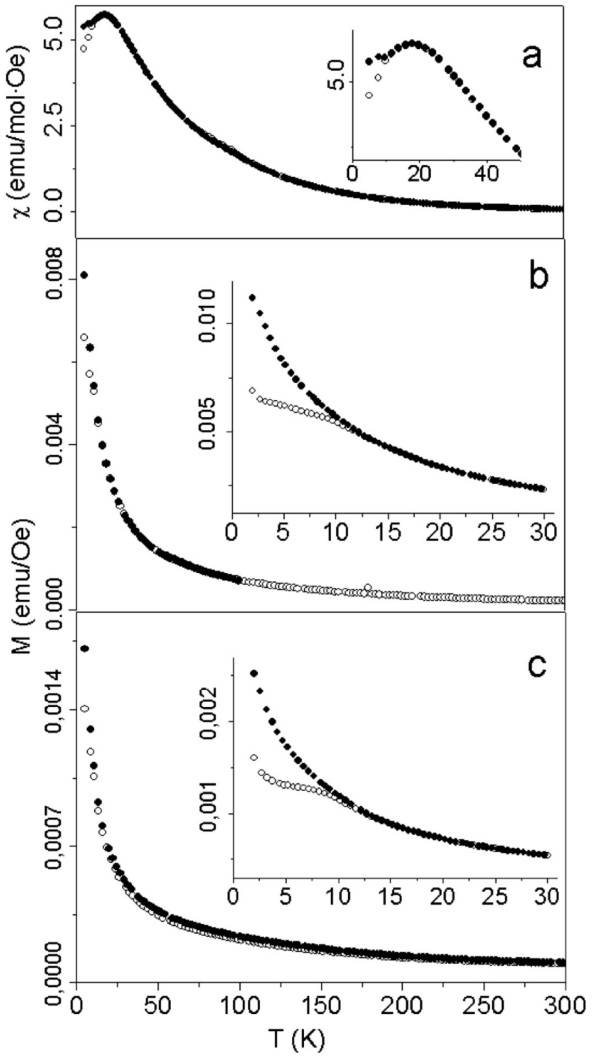

Figure 5. ZFC and FC susceptibility for Zn3 sample (a) and magnetization vs temperature for SZn (b) and FZn (c) samples with an applied magnetic field of 500 Oe.

calculated using the BJH method is plotted in Figure 4b. In the inset is depicted the pore size distribution in both micropores and mesopores regions. The frontier between both regions has been indicated by a vertical dotted line. In the micropores region it can be seen for both samples a sharp increase of the cumulative volume for a pore diameter of 1.3 nm which corresponds to the supercage diameter (see the inset). These results suggest that the faujasite structural micropores are partially occupied by ferrite nanoparticles. As in the case of the SZn sample, the particles ranging from 1 to 3 nm that can be seen in the micrographs (Figure 2c,d) must be located in larger pores that probably correspond to the structural defects. According to that, the mesopore volume is lower for the FZn sample (see Table 1).

It can be seen in Figure 5a the ZFC and FC magnetic susceptibility measured at 500 Oe for the Zn3 sample. The magnetization vs temperature was also measured at 500 Oe for the SZn and FZn samples shown in parts b and c of Figure 5, respectively. While the nonencapsulated nanoparticles (Zn3 sample) present a T_B value of 18 K that corresponds to the maximum of the ZFC magnetic susceptibility, the T_B for entrapped particles into sepiolite and faujasite

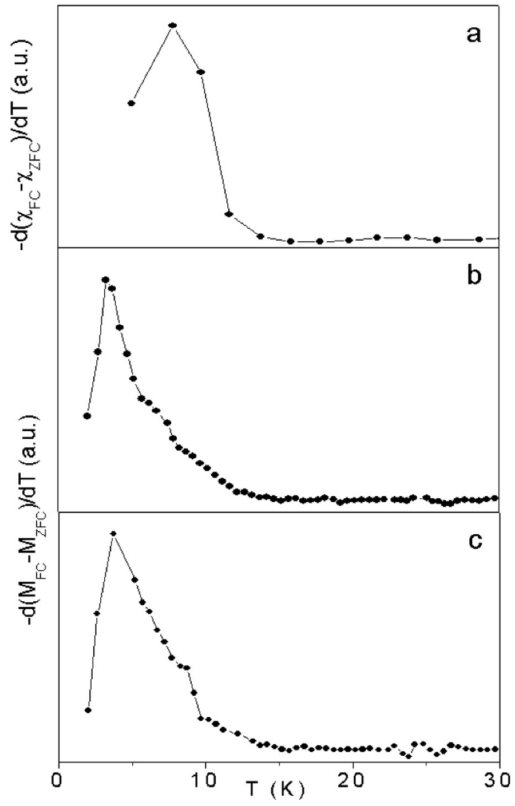

Figure 6. Blocking temperature distribution obtained from the derivative $d(\chi_{ZFC} - \chi_{FC})/dT$ of experimental data for Zn3 sample (a), and derivative of $d(M_{FC} - M_{ZFC})/dT$ of experimental data for SZn (b) and FZn (c) samples that reflect the particle size distribution.

matrixes (SZn and FZn samples, respectively) seems to be below 5 K as the maximum of the ZFC curve has not been reached yet, although a plateau is observed in both cases (see inset of Figure 5a,b). On the other hand, the well-known Néel expression of the relaxation time of a superparamagnetic particle[35] $\tau_m = \tau_0 \exp(E_a/k_B T)$ and the expression $E_a = KV$ establish a relation between the T_B and the particle size. τ_m is the measuring time, τ_0 is the characteristic time, K is the magnetic anisotropy constant, V is the particle volume, and k_B is the Boltzmann constant. Thus, from the derivative of $(M_{FC} - M_{ZFC})/dT$ it has been determined the T_B distribution for each sample (see Figure 6), which in addition reflects the particle size distribution.[36] In the case of the Zn3 sample, the slightly broader maximum that can be seen around 8 K (Figure 6a) indicates a wider particle size distribution than for the encased nanoparticles in both matrixes (Figure 6b,c). The fact that the 8 K peak of this maximum does not match with the T_B value of 18 K reveals that the system is not completely homogeneous.[37] Although the T_B distribution of the SZn and FZn samples show a sharp peak, it can be observed a widening on their right size. This may indicate the presence of two well-defined particle sizes, with the majority the smallest particles which are probably located in the micropores. The minority would correspond to the largest particles which may be hosted in the structural defects of the matrixes. These results agree well with those previously described, obtained from the adsorption study. Thus, from the ZFC curve of SZn and FZn samples (Figures 5a,b), it can be understood that the largest particles present a T_B around 8 K while the smallest ones, supposed to be entrapped in the microstructural pores, have not reached their T_B when the temperature is lowered down to 2 K as it can be deduced from the ascending trend of the ZFC curve. On the other hand, unlike the nanoparticles encased in both sepiolite and faujasite matrixes, free of matrix nanoparticles present particle interactions as the decreasing shape of the FC curve seems to indicate when the temperature decreases from the T_B. This reveals the useful role that the matrixes play when they are used as structures in which disperse nanoparticles. It is also worth noting the different shape that the ZFC and FC curves adopt in the temperature range of 5−300 K, depending on whether the nanoparticles are encased in a matrix or not. Thus, while free of matrix nanoparticles (Figure 5a) show a smooth decreasing susceptibility from T_B to approximately 150 K which implies a high magnetic response, when they are encapsulated (Figure 5b,c) the mentioned curves show an abrupt decrease of the magnetization with the increasing of the temperature. The Zn3 sample shows a typical superparamagnetic behavior from T_B until approximately 150 K. Above this temperature, the onset of the paramagnetic behavior takes place as it will be discussed later. In the superparamagnetic region, the thermal energy is higher than the anisotropy energy and, therefore, gradually it starts to avoid the magnetic order imposed by the applied field. However, in the case of the encased nanoparticles (SZn and FZn samples), the thermal energy seems to be more effective as a sharp decreasing in the magnetization is observed after reaching the T_B. This can be justified under the consideration that the encased nanoparticles are free to rotate accompanying the reversal of their magnetic moments induced by the thermal energy.[23] The achieved free rotation may be due to the good dispersibility of the nanoparticles in the cavities of the host-matrixes and to the absence of any local mechanical impediment imposed by the host-structure.

The reciprocal susceptibility as a function of the temperature for Zn3 sample is depicted in Figure 7a. Figure 7b,c shows the inverse of the magnetization vs the temperature for SZn and FZn samples, respectively. While the Zn3 sample presents a gradual transition from superparamagnetic to paramagnetic behavior (see Figure 7a), in the case of encapsulated nanoparticles (SZn and FZn samples), the data could be fitted to two straight lines with very similar slopes. The temperature at which the nanoparticles start to behave as paramagnetic seems to be around 150 K indicated by the end of Curie−Weiss behavior for the superparamagnetic temperature range in the case of the Zn3 sample. This transition temperature from superparamagnetic to paramagnetic behavior cannot be visualized in the M^{-1} vs T plots in the case of the SZn and FZn samples because both behaviors present very similar slopes. This can be justified under the consideration of the importance that the surface

(35) Néel, L. *Ann. Geofis.* **1949**, *5*, 99.
(36) Denardin, J. C.; Brandl, A. L.; Knobel, M.; Panissod, P.; Pakhomov, A. B.; Liu, H.; Zhang, X. X. *Phys. Rev. B* **2002**, *65*, 064422.
(37) Lu, J. J.; Huang, H. L. *Chin. J. Phys.* **2000**, *38*(2-I), 97.

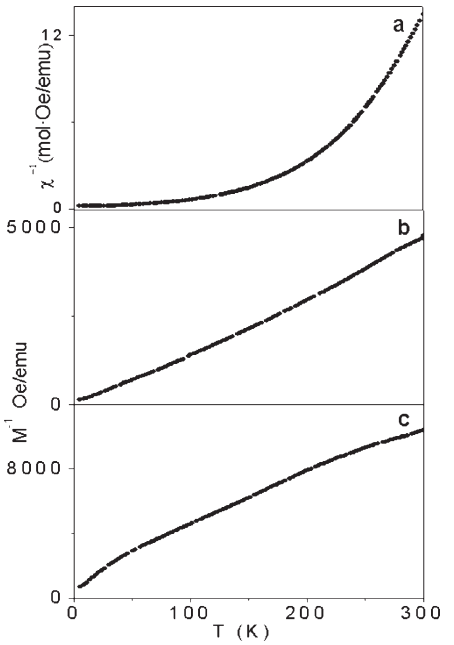

Figure 7. Inverse of ZFC susceptibility for Zn3 sample (a) and inverse of magnetization vs temperature for SZn (b) and FZn (c) samples.

phenomena acquire when the particle size is very small. Considering that most of the particles in the nanocomposites are confined in the micropores, the spin-canting present in the surface of these nanoparticles would make almost negligible the moment corresponding to the particle core.

Hysteresis loops at 5 K for nonencapsulated and encapsulated nanoparticles are shown in parts a, b, and c of Figure 8, respectively. Free of matrix nanoparticles present a characteristic loop of a ferrimagnetic behavior with a coercive field (H_C) of 106 Oe. However, when these nanoparticles are encased into sepiolite or faujasite matrixes, they present a H_C value of 180 and 185 Oe, respectively, which may correspond to the largest particles hosted in the structural defects as they present a T_B around 8 K. This difference in coercivity can be attributed to two main factors: (i) different inversion degree of the ferrite nanoparticles and (ii) different surface anisotropy that seems to control the H_C value.[38] However, taking into account that the solvothermal method was used in the preparation of both kind of samples, encapsulated and free of matrix nanoparticles, (Zn3, SZn, and FZn), presumably, nonencapsulated and encapsulated ferrite particles present a very similar inversion degree. Then, the most powerful reason to explain this difference in coercive values could be a different surface anisotropy depending on whether the particles are hosted or not in a matrix. An example of surface anisotropy modification can be found in a previous work[22] where it has been demonstrated that the strain imposes by a solid SiO_2 matrix provokes until 1 order of magnitude higher values of H_C for the embedded ferrite nanoparticles. In the case of the SZn and FZn samples, the matrix structures do not seem to impose any strain as the nanoparticles are free to rotate. The slightly higher values of

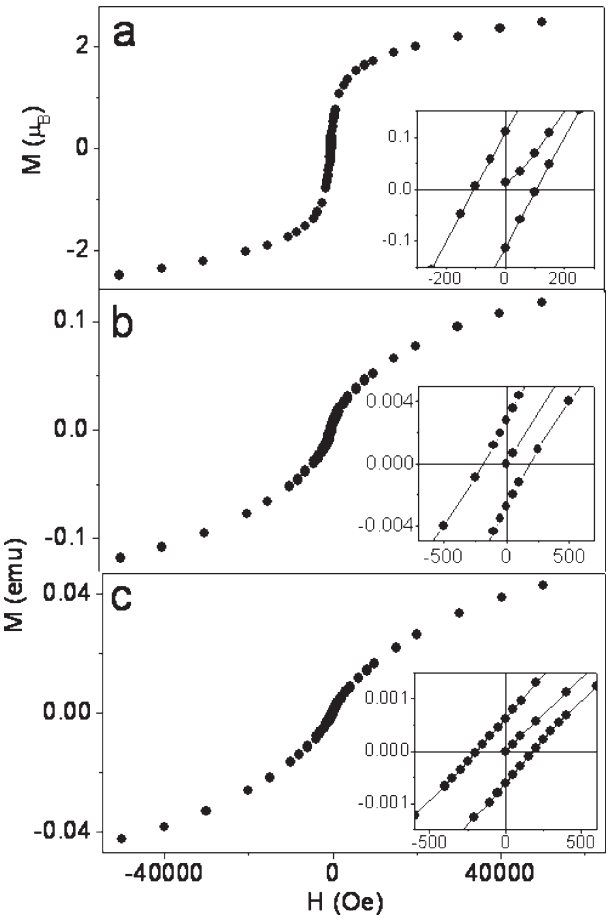

Figure 8. Hysteresis loops measured at 5 K for Zn3 (a), SZn (b), and FZn (c) samples. The insets show a detail of the loops.

H_C for hosted nanoparticles in sepiolite and faujasite could be attributed then to the absence of interparticle interaction as a consequence of the good dispersibility achieved in the matrixes.[39] Thus, unlike these hosted particles, in the case of the Zn3 sample, the particle interaction may slightly decrease the surface anisotropy resulting in a lower value of H_C.

4. Conclusions

Zn-ferrite nanoparticles have been obtained dispersed in the micropores and mesopores of sepiolite and faujasite matrixes using a simple method of wet impregnation followed by a solvothermal treatment. The particle size distribution shows two well-defined sizes for the entrapped nanoparticles in sepiolite and faujasite matrixes. The adsorption data suggest that the smallest particles must be entrapped in the micropores of the matrixes while the largest ones may be hosted in mesopores corresponding to structural defects. The magnetic data indicate that the nanocomposites may contain rotationally free hosted-particles. Thus, the abrupt decreasing of magnetization with the temperature above the blocking temperature leads one to believe that the nanoparticles easily accompany the reversal of the magnetic moment with their rotation when the thermal energy overcomes the magnetic order imposed by

(38) Vestal, C. R.; Zhang, Z. J. *J. Am. Chem. Soc.* **2003**, *125*, 9828.

(39) Zhu, Y.; Zhao, W.; Chen, H.; Shi, J. *J. Phys. Chem. C* **2007**, *111*, 5281.

the external field. On the other hand, the temperature ranges in which the sample behaves as superparamagnetic and paramagnetic are more clearly defined when they are not encased into sepiolite and faujasite matrixes. In comparison to free of matrix nanoparticles, the hysteresis loops at 5 K show slightly higher values of H_C in the case of entrapped nanoparticles. This can be attributed to the absence of interparticle interaction due to the good dispersibility of these nanoparticles in the matrixes.

Acknowledgment. The authors are grateful to the Ministerio de Ciencia e Innovación for financial support under Project MAT 2007-63497, Universidad Complutense de Madrid for a predoctoral grant and Nubiola Pigments. The authors also thank to "Centro de Microscopía Electrónica" and "CAI de difracción de Rayos X" at UCM for technical assistance.

Supporting Information Available: TG-curve for sepiolite and TEM images of S350s and Fs samples (PDF). This material is available free of charge via the Internet at http://pubs.acs.org.